RSC Advances

ROYAL SOCIETY OF CHEMISTRY

www.rsc.org/advances

RSC Advances

RSCPublishing

PAPER

Superior methanol electrooxidation activity and CO tolerance of mesoporous helical nanospindle-like CeO_2 modified Pt/C

Cite this: DOI: 10.1039/x0xx00000x

Received ooth January 2012,
Accepted ooth January 2012

DOI: 10.1039/x0xx00000x

www.rsc.org/

Jing Chen, Songmei Li*, Juan Du, Jianhua Liu, Mei Yu, Shiming Meng and Bo Wang

In an attempt to enhance electrocatalytic activity and CO tolerance of ceria modified Pt/C electrode, a novel structured ceria has been developed. Left-handed helical CeO_2 nano-spindles with mesoporous structures are successfully synthesized through a template-free based precursor method in large scale. By a microwave-assisted polyol synthesis process, ceria modified Pt/C electrocatalysts are synthesized. The helical CeO_2 nanospindle based electrode Pt@Heli-CeO_2/C exhibits superior electrochemically active surface areas, significantly enhanced methanol oxidation catalytic activity and CO antipoisoning activity, compared to Pt/C and nano-octahedral CeO_2 modified electrode Pt@Octa-CeO_2/C. The experimental results show that Pt@Heli-CeO_2/C possesses 8.2 times and 3.2 times higher activity for methanol electrooxidation than Pt/C and Pt@Octa-CeO_2/C, respectively. This remarkable enhancement could be attributed to reasons as follows: compared to octahedral CeO_2, unique helical CeO_2 is more conductive to electron transfer and can provide more active surface sites to strengthen the support-metal interactions based on electronic transfer mechanism from CeO_2 to Pt, thus helical CeO_2 can promote better dispersion of Pt (0) nanocrystallites and high concentration of metallic Pt (0) composition.

Introduction

Direct methanol fuel cells (DMFCs) are gaining attractive attention as promising power storage device for electric vehicle and portable power applications for decades,[1-3] due to their unique properties, such as low operating temperature, low emission of pollutants and relatively high energy density.[4] However, intermediates during the anodic oxidation processes, especially carbon monoxide, will poison platinum based catalyst and lead to low methanol oxidation activity at the anode. To mitigate CO poisoning, one solution is to design Pt-based bimetallic or trimetallic catalysts, a number of multi-alloyed electrocatalysts, such as PtSn,[5, 6] PtRu,[7, 8] PtRh,[9, 10] PtCu,[11] PtRuIr,[12] and PtRuNi[13] have been precisely fabricated. Another strategy is to use transition metal oxides supported or modified electrocatalyst, such as Pt/SnO_2,[14] Pt/TiO_2,[15, 16] Pt/SiO_2,[17] based on multi-functional mechanism[18] and electronic modification.[19]

In particular, CeO_2 is considered to be a potential co-catalyst because of its high oxygen storage capacity and anticorrosion ability in acidic media, especially for alcohol oxidation. It was reported that ceria modified Pt/C electrocatalyst exhibited enhanced methanol oxidation activity compared with that of Pt/C[20] or PtRu/C.[21, 22] However, low electron transfer rate of CeO_2 together with the weak interaction between CeO_2 and Pt, still limit its catalytic performance. Until now, many efforts have focused on structure designing and doping of CeO_2-modified electrocatalysts to improve the synergistic effect and electronic conductivity. Du et. al.[23] developed a Pd-surrounded-CeO_{2-x} catalyst via a three-phase-transfer approach, and it exhibited an excellent catalytic performance for methanol oxidation attributed to enhanced interfacial interaction between

CeO_{2-x} and Pd. Chu[24] and co-workers synthesized nitrogen doped carbon packed Pt/CeO_2 catalyst via in situ carbonization of ionic liquid, and it exhibited greatly enhanced electrical conductivity of the CeO_2. But fewer papers have focused on new structure design of CeO_2 to enhance the electron conduction. It was found that, the configurations of metal oxide played critical roles in the electronic structure[16, 25, 26] and the synergetic interaction between metal oxide and Pt.[4, 27] Therefore, it is useful to explore novel morphology of CeO_2 as a cocatalyst in methanol electrooxidation.

The helical structured materials, exhibited sophisticated morphology as well as unique chemical and physical activity, are usually associated with biological polymers or organic materials.[28] Inorganic materials with helical nanostructure have not been widely explored.

In this investigation, when L-AspNa was used as an additive, uniform helical spindle-like cerium compound was successfully fabricated through the interaction among the additives (L-AspNa), precipitating agent (Na_2CO_3), and inorganic source ($Ce(NO_3)_3$•$6H_2O$). After a thermal decomposition, the mesoporous nanospindle-like CeO_2 polycrystal with a helical architecture was produced. This helical nanospindle-like CeO_2 based catalyst displayed 8.2 fold enhancement of methanol oxidation performance compared to Pt/C.

EEPERIMENTAL SECTION

Synthesis of Ceria Nanostructures

All chemicals used are purchased from chemical CO., LTD. directly. In the synthesis of helical CeO_2, 2 mmol $Ce(NO_3)_3$•$6H_2O$ was dissolved in 10 ml 0.6 M AspNa solution, then 10 mL 0.15 M Na_2CO_3 was dropped to the above solution and stirred vigorously at ambient condition for 3 h. After that, the resulting white turbid liquid was poured into a 30 mL Teflon-lined stainless autoclave and treated at 160 ^oC for 24 h. The obtained products were washed with deionized water and ethanol twice, then stay overnight at 60 ^oC in air, named as Heli-CeO_2-P. Then Heli-CeO_2-P was calcined under air condition at 350 ^oC for 3 h, to get helical structured ceria (named as Heli-CeO_2).

For the preparation of CeO_2 nano-octahedron (Octa-CeO_2), all the other experimental procedures remained the same as described above, except for the absence of amino acids and further calcination.

Characterization

X-ray diffraction (XRD) data was recorded by Rikagu D/max 2200PC , with Cu Kα radiation (λ=1.5406 Å). Thermogravimetry-differential thermal (TG-DTA) curves were obtained on a NETZSCH instrument DSC/TGA-STA 449F3 in air at a heating rate of 10 ^oC min^{-1}, using α-Al_2O_3 as a reference. Filed-emission scanning electron microscopy (FESEM) observations were employed by FEI SIRION microscope. Transmission electron microscopy (TEM), high-resolution TEM (HRTEM), and selected-area electron diffraction (SAED) were collected on a JEOL 2010 FEG microscope at 200 kV. N_2 adsorption–desorption isotherms and Brunauer Emmett Teller (BET) surface areas of nanostructured ceria samples were recorded on a BELSORP-mini II sorption instrument at 77 K. H_2-Temperature-programmed reduction (TPR) was performed on a Quantachrome ChemBET 3000 analyzer at rate of 10 ^oC min^{-1} using 10% H_2/Ar mixed gas with a flow of 25 ml min^{-1}. X-ray photoelectron spectroscopy (XPS) was determined using a PHI-Quantera SXM.

Preparation of Electrocatalyst Composites.

Electrocatalysts were prepared as reported in the literature.[29] Firstly, a liquid mixture of ethylene glycol (EG) and isopropyl alcohol with a volume ratio of 4:1 was prepared. Secondly, 5 mg CeO_2 and 20 mg carbon powder were dispersed into above solution with ultrasonication until a homogeneous mixture was formed. After adding 5.85 mL of 0.01 M H_2PtCl_6-EG into the above mixture, 0.8 M KOH-EG was used to adjust the pH to 10 dropwise. After stirring for another 6 h, the resulting mixture was heated in a domestic microwave oven (750 W, Galanz, China) for 50 s. After cooling to room temperature, 15 mL 0.1 M HNO_3 was dropped to adjust the pH to ~4 with vigorous stirring for 12 h, the resulted black suspension was centrifuged and washed with distilled water and ethanol twice. The product was then dried at 40 ^oC for 12 h in vacuum drying oven. To evaluate the role of ceria, Pt/C electrocatalyst was also synthesized using similar procedure, but without CeO_2. It is very easy to reproduce Pt nanoparticles by this microwave method. The repeated catalysts was named as Pt@Heli-CeO_2/C-re1, Pt@Heli-CeO_2/C-re2, Pt@Octa-CeO_2/C-re1, Pt@Octa-CeO_2/C-re2, Pt/C-re1 and Pt/C-re2, the results were shown in supporting information.

Electrochemical Measurements

Electrochemical measurements were all tested on Princeton VMC-4 potentiostation with a conventional three-electrode system (working electrode: glassy-carbon electrode (GCE) with diameter 6 mm, reference electrode: an Ag/AgCl electrode and counter electrode: Pt wire) at room temperature. 5 mg Pt/C, Pt@Heli-CeO_2/C or Pt@Octa-CeO_2/C composite powders, were re-dispersed in 1.0 mL isopropanol under sonication, then 0.1 mL Nafion solutions (0.5 wt%) was added to form catalytic ink. To prepare working electrode, 10 uL catalyst inks were dropped on a polished mirror GCE using a pipette and dried at room temperature. Prior to electrochemical measurements, the electrolytes were deoxygenated with N_2 for 30 min.

The cyclic voltammogram (CV) was recorded in 3 mL 0.5 M H_2SO_4 and 3 mL 2 M CH_3OH solution, from 0 to 1.0 V at 50 mV s^{-1} until a steady CV was obtained. Chronoamperogram (CA) measurement was carried out at 0.5 V for 3600 s in 0.5 M H_2SO_4 and 2 M CH_3OH. CO stripping voltammetry and electrochemical active surface areas (ECSA) of platinum were performed in 0.5 M H_2SO_4 at 20 mV s^{-1}. Prior to CO adsorption, the system was deoxygenated by bubbling with N_2 for 30 min. And then at -0.1V CO (10% CO in Ar balance) was adsorbed onto the electrodes by bubbling CO gas for 10 min.

To remove any dissolved CO, N_2 was purging for another 15 min. Then the adsorbed CO was oxidized from -0.2 V to 1.1 V by CV. The ECSA of platinum was calculated with the formula $ECSA_{pt} = Q_H/(0.21 \cdot M_{Pt})$.[30-32] Electrochemical impedance spectroscopy (EIS) was performed during frequency range 0.01-100kHz with 30 points per decade.

Result and discussion

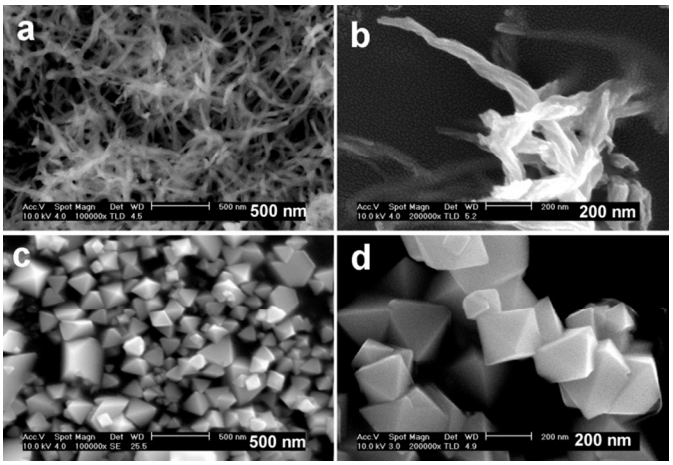

Figure 1. SEM images of CeO_2 with (a, b) helical spindle and (c, d) nano-octahedrons morphologies.

With and without L-AspNa, two products were prepared via hydrothermal treatment of $Ce(NO_3)_3$ (aq.) and Na_2CO_3 (aq.) mixture. The morphologies and sizes of these two cerium compounds were investigated SEM, as shown in Figure 1. Figure 1a presents the picture of cerium precursors synthesized with the help of L-AspNa. Most of the products in this picture present a unique spindle-like morphology. At high magnification (Figure 1b), left-handed helical structure, named Heli-CeO_2-P, can be observed distinctly. The spiral diameter ranges from 40 to 100 nm. In contrast, if the sample was synthesized without L-AspNa, the compound consists of regular octahedron particles, as shown in Figure 1c and 1d. This structure, with a smooth surface and edge length ranging from 100 to 600 nm, is named Octa-CeO_2. SEM results indicate that when L-AspNa was used as an additive, the products morphology can be obviously changed from nano-octahedron to nano-spindle.

XRD results of the two cerium compounds are exhibited in Figure 2, Octa-CeO_2 (Fig 2 blue line) is face-centered cubic CeO_2 (JCPDS Card No. 65-5923). The strong diffraction peaks at Bragg angles of 28.4°, 33.3°, 47.6°, 56.3°, 59.1°, 69.4°, 76.7°, and 79.1° can be assigned to (111), (200), (220), (311), (222), (400), (331), and (420) crystal planes, respectively. However, Heli-CeO_2-P is amorphous from XRD measurement (Fig 2, black line). These results imply that, not only the morphology, but also the crystalline process of the precursor was affected by the addition of L-AspNa. Additionally, TG-DTA was performed to confirm complete decomposition temperature of Heli-CeO_2-P. TG-DTA results (see Figure S1) show that 350 °C

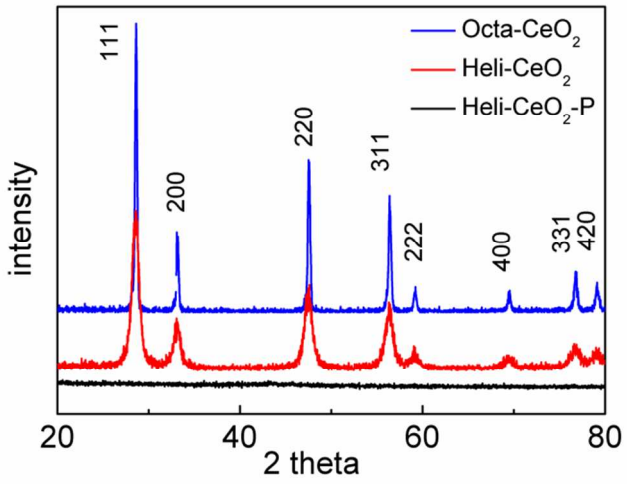

Figure 2. XRD patterns of cerium compounds with different morphologies.

was the minimal temperature to obtain pure CeO_2 from the amorphous precursor. The XRD pattern of the yellowish ceria power obtained after calcinating, named Heli-CeO_2, is presented in Figure 2 (red line). The existence of the narrow and intense diffraction peaks indicates the structure of cubic CeO_2.

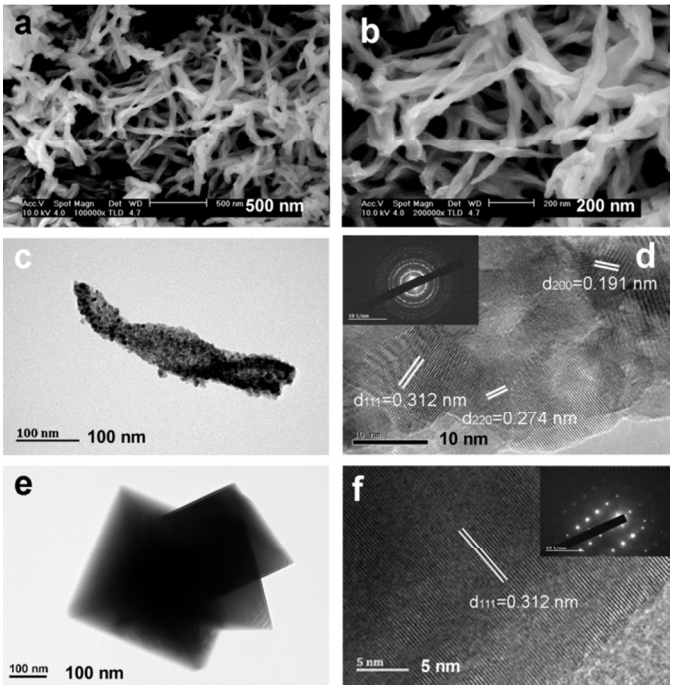

Figure 3. SEM (a,b) and TEM (c,d) images of helical spindle-like CeO_2, TEM images (e,f) of nano-octahedrons CeO_2.

A closer inspection of the SEM result of Heli-CeO_2 (Figure 3a) shows ceria nanospindles with a fair uniformity. The helical structure was well preserved after calcination. SEM (Figure 3a and b) and TEM (Figure 3c) images, suggest the presence of tip at each end of a CeO_2 nanospidle. The length of Heli-CeO_2 is approximately 900 nm, and the diameter of the widest part of

Heli-CeO_2 is around 90 nm. A closer examination of one helical spindle-like Heli-CeO_2 (Figure 3d) indicates nanoparticles, with diameters of about 8 nm, as the building blocks for Heli-CeO_2. This was also confirmed by SAED patterns (inset in Figure 3d) of Heli-CeO_2, which shows a polycrystalline diffraction pattern. In Figure 3d, the interplanar spacing of lattice fringes (111), (200) and (220) were identified to be 0.312, 0.274 and 0.191 nm, respectively. TEM image in Figure 3e, confirmed fairly perfect nano-octahedron morphology with clear edges and corners on Octa-CeO_2. HRTEM image in Figure 3f displays clear (111) planes with fringe spacing of 0.312 nm. The corresponding SAED pattern (inset in Figure 3f) showed typical single crystalline structure of the Octa-CeO_2 sample. N_2 adsorption/desorption isotherms (shown in Figure S2) confirmed different porous structures for Heli-CeO_2 and Octa-CeO_2: while there were mesopores accumulated by the nanoparticles within the helical spindle-like structure, the porous structure was not present in Octa-CeO_2. Correspondingly, Heli-CeO_2 owns much larger specific surface area (~27 m^2 g^{-1}) than Octa-CeO_2 (~2 m^2 g^{-1}). H_2-TPR results reveal that helical spindle Heli-CeO_2 sample shows two highly intense low-temperature reduction peaks at 421 °C and 445 °C, whereas, nano-octahedron Octa-CeO_2 shows one reduction peak at 508 °C. This difference demonstrates that helical spindle Heli-CeO_2 is much more reducible and active than the nano-octahedron Octa-CeO_2 materials (Figure S3).

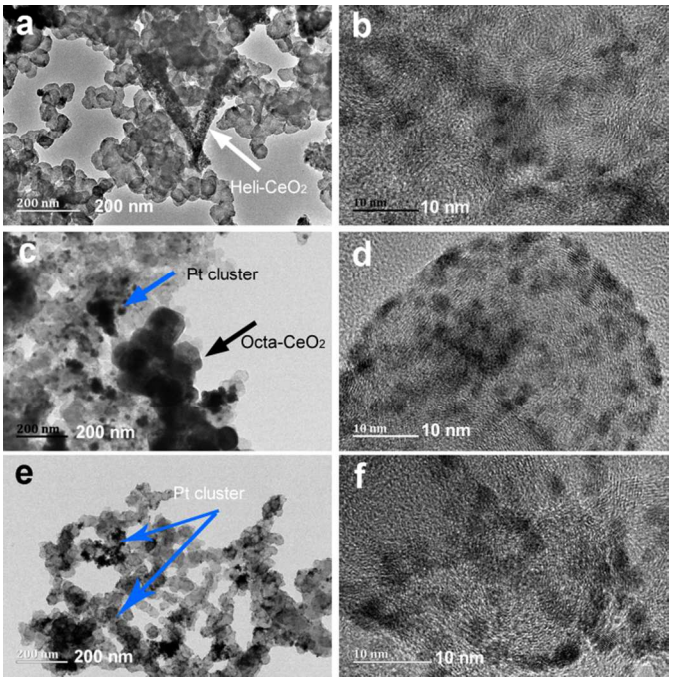

Figure 4. TEM images of (a,b) Pt@Heli-CeO_2/C, (c,d) Pt@Octa-CeO_2/C. (e,f) Pt/C

Ceria promoted Pt/C electrocatalysts were prepared by a microwave-assisted polyol synthesis method , and TEM images of the electrocatalysts are exhibited in Figure 4. In the case of Pt@Octa-CeO_2/C and Pt/C, the distribution of Pt nanoparticles is not as uniform as Pt@Heli-CeO_2/C, and large Pt clusters are detected on selected surface of Octa-CeO_2 supported carbon black (Figure 4c) and bare carbon black (Figure 4e), respectively. On the other hand, the helical spindle-like Heli-CeO_2 supported carbon black significantly improves the dispersion and distribution of Pt nanoparticles, as presented in Figure 4a. The average diameters of Pt nanoparticles with well-defined fingerprints (Figure 4b, 4d, 4f) in Pt@Heli-CeO_2/C, Pt@Octa-CeO_2/C and Pt/C are about 2.2, 2.2 and 2.5 nm, respectively. The repeated results are shown in Figure S4. Helical spindle-like Heli-CeO_2, with high concentration of active crystal face ((220) and (200)) and oxygen vacancies, offers a stronger metal-support interaction between Heli-CeO_2 and Pt nanoparticles based on electronic transfer mechanisms.[18, 32-33] Therefore, the surface electronic properties of Pt were modified, attributed to a shift in the d-band center of the surface Pt atoms, inducing a higher concentration of metallic Pt (0). Furthermore, the stronger interaction between Pt nanoparticles and helical spindle-like Heli-CeO_2 can prevent agglomeration of Pt nanoparticles; form highly dispersed and stable Pt nanoparticles.

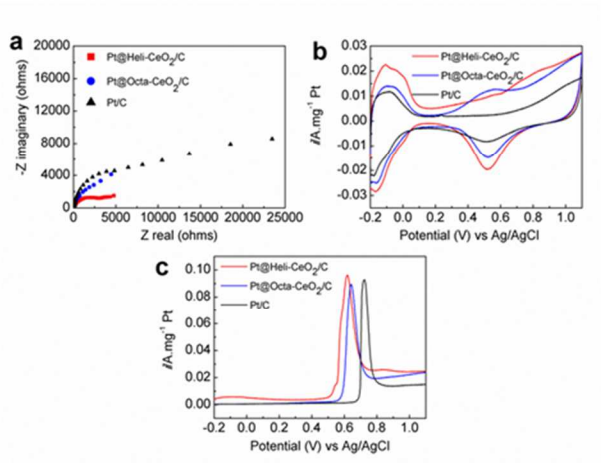

Figure 5. (a) The electrochemical impedance spectra (EIS) in 0.5M H_2SO_4 and 2M CH_3OH, and (b) CVs in 0.5 M H_2SO_4 at 20 mV s^{-1}, (c) CO stripping voltammograms in 0.5 M H_2SO_4 at 20 mV s^{-1} of Pt@Heli-CeO_2/C, Pt@Octa-CeO_2/C and Pt/C.

To understand the role of helical CeO_2-H in enhancing the catalyst conductivity, electrochemical impedance spectrascopy (EIS) is carried out. As shown in Figure 5a, the same pattern appears and the semicircle of Pt@Heli-CeO_2/C is much smaller than Pt@Octa-CeO_2/C and Pt/C, reflecting that the impedance of helical ceria modified Pt@Heli-CeO_2/C is reduced significantly compared with octahedron ceria modified Pt@Octa-CeO_2/C and Pt/C.[33, 34] This remarkable enhancement in electron transmission may be attributed to the helical structure, which is more conductive to electron transfer than that of the corresponding octahedral structures.[35, 36] The electrochemical surface characteristics of the Pt@Heli-CeO_2/C are compared with Pt@Octa-CeO_2/C and Pt/C catalysts using cyclic voltammetry (Figure 5b). As shown in the black curve for Pt/C electrocatalyst, platinum oxide formation/reduction peaks is less obvious, ascribed to the aggregation of Pt and corrosion of the carbon powder.[37] In contrast, when ceria is added, Pt oxide formation/reduction peaks is distinctly visible.

In addition, the voltammogram of Pt@Octa-CeO_2/C exhibits similar double layer charging current and hydrogen adsorption/desorption peaks to that of Pt/C catalyst. The similar features of Pt@Octa-CeO_2/C and Pt/C indicate that the interaction between octahedron Octa-CeO_2 and Pt nanoparticles in Pt@Octa-CeO_2/C is not strong. However, for Pt@Heli-CeO_2/C, the hydrogen adsorption/desorption peak becomes broader and more noticeable, and the double layer charging current becomes larger, compared with that of octahedron ceria modified Pt@Octa-CeO_2/C and Pt/C, implying a stronger interfacial interaction between Heli-CeO_2 and Pt.[38] The ECSA of Pt@Heli-CeO_2/C estimated from the hydrogen adsorption peaks is 80.95 m^2 g^{-1}, which is almost two times larger than that of Pt@Octa-CeO_2/C and Pt/C (47.16 m^2 g^{-1} and 40.67 m^2 g^{-1}, respectively). This is attributed to the improvement in electron conductivity, highly dispersed and multifaceted Pt crystallites on the helical spindle-like Heli-CeO_2 promoted Pt/C elecrocatalyst.

Figure 5c presents the CO_{ad} stripping curves of Pt@Heli-CeO_2/C, Pt@Octa-CeO_2/C and Pt/C. As shown in Figure 5c, the CO onset and peak oxidation potential are 0.5, 0.53, 0.68 V and 0.62, 0.64, 0.72 V for Pt@Heli-CeO_2/C, Pt@Octa-CeO_2/C and Pt/C, respectively. The comparison indicates that nano-shaped ceria promoted Pt/C electrocatalysts present lower oxidation potentials and broader CO_{ad} oxidation peaks, with helical nanospindle Heli-CeO_2 promoted Pt/C, showing the highest CO oxidation activity among these three electrocatalysts. The helical morphology of Heli-CeO_2, possessed more active crystal facets and oxygen vacancies, could increase the synergic interaction and intimate contact between the interface of Pt and oxygen-containing species of helical structured Heli-CeO_2 due to electronic transfer mechanisms.[19] The OH groups generated on the surface of Heli-CeO_2, react with absorbed CO on Pt particles, and then produce CO_2.[39]

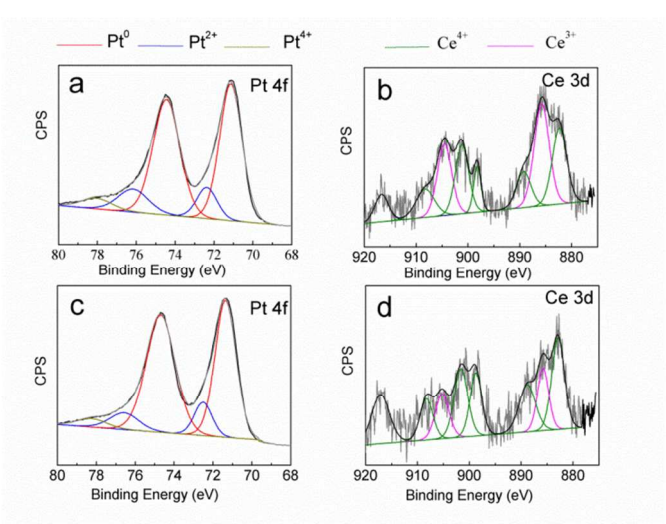

Figure 6. (a) Pt 4f and (b) Ce 3d core-level XPS spectra of Pt@Heli-CeO_2/C samples. (c) Pt 4f and (d) Ce 3d core-level XPS spectra of Pt@Octa-CeO_2/C samples.

To investigate the interaction between nanostructured ceria and platinum nanoparticles in the as-prepared electrocatalyst, XPS spectra were measured to obtain their chemical and electronic information. The Pt 4f and Ce 3d XPS data of Pt@Heli-CeO_2/C and Pt@Octa-CeO_2/C are shown in Figure 6, and the deconvoluted results are summarized in Table 1. The Pt 4f spectra are deconvoluted into 5 peaks, including three Pt chemical states: Pt (0), Pt (II), and Pt (IV).[40-42] For Pt@Heli-CeO_2/C, the Pt 4f binding energy of Pt (0) peaks show a larger shift to lower energies by about 0.3 eV, whereas Pt (0) peaks shows only 0.1 eV shift for Pt@Octa-CeO_2/C compared to Pt/C,

Table 1. Binding energies and relative intensities of various species as obtained from the Pt-4f and Ce-3d X-ray photoelectron spectra of Pt/C, Pt@Heli-CeO_2/C and Pt@Octa-CeO_2/C.

Sample	peak	species	binding energy (eV)						relative ratio
Pt/C	Pt 4f	0	71.7	75.0					76.9
		+2	73.1	76.5					18.9
		+4	78.3						4.2
Pt@Heli-CeO_2/C	Pt 4f	0	71.4	74.7					79.1
		+2	72.6	76.4					16.8
		+4	78.3						4.1
	Ce 3d	+3	886.0	904.7					40.5
		+4	882.5	889.7	898.4	901.3	908.4	916.9	59.5
Pt@Octa-CeO_2/C	Pt 4f	0	71.6	74.9					62.5
		+2	72.7	76.8					33.3
		+4	78.2						4.2
	Ce 3d	+3	886.0	905.2					21.8
		+4	882.9	888.9	898.9	901.8	908.4	917.1	78.2

and this can be attributed to a much stronger interaction between Pt and helical structured Heli-CeO_2.[39, 43, 44] Moreover, the metallic Pt species in Pt@Heli-CeO_2/C, Pt@Heli-CeO_2/C, and Pt/C, is estimated to be 79.1, 62.5 and 76.9 %, respectively. The relatively high ratio of metallic Pt will be beneficial for high catalytic performance.[40] In addition, Ce 3d XPS spectra reveal three-lobed envelopes (around 878–895 eV, 895–912 eV and approximately 917 eV) such as those depicted in Figure 6b and d. The Ce 3d spectra are deconvoluted into 8 peaks.[45] The percentage of Ce (III) relative to the total amounts of Ce is estimated to be 40.5 and 21.8% for Pt@Heli-CeO_2/C and Pt@Octa-CeO_2/C catalysts, respectively. The higher

concentration of Ce (III) in Heli-CeO_2 modified Pt/C catalysts are owe to the smaller size of the constituent ceria nanoparticles, which possess a higher proportion of surface defects. The obvious differences in Ce (III) relative intensities between Pt@Heli-CeO_2/C and Pt@Octa-CeO_2/C could have great impact on the reducibility of Pt species. This is supported by the analysis of the Pt 4f spectrum,[46] showing the Pt (0) relative intensity of 79.1 and 62.5% for Pt@Heli-CeO_2/C and Pt@Octa-CeO_2/C. XPS data show that Pt@Heli-CeO_2/C catalyst has 40.5 % Ce (III) species, which would give rise to higher activity oxygen; moreover, due to a stronger interaction between helical structured Heli-CeO_2 and Pt particles, much more Pt species can be easily reduced to Pt (0).

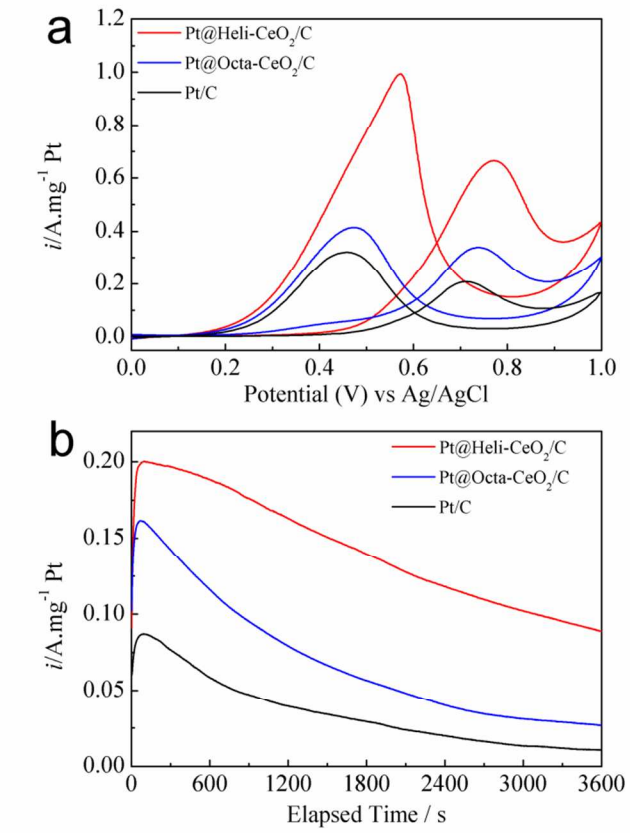

Figure 7. (a) CVs measured in 0.5 M H_2SO_4 and 2 M CH_3OH, 50 mV s^{-1}; (b) Chronoamperometry curves measured in 0.5 M H_2SO_4 and 2 M CH_3OH solution fixed at 0.5 V, 50 mV s^{-1} of Pt@Heli-CeO_2/C, Pt@Octa-CeO_2/C Pt/C.

Voltammetric curves in N_2 saturated 0.5 M H_2SO_4 and 2.0 M CH_3OH aqueous solution are shown in Figure 7a.[47, 48] Evidently, current densities at the maximum in the forward sweep of these electrodes are, in order, Pt@Heli-CeO_2/C (0.99 A mg^{-1} Pt) > Pt@Octa-CeO_2/C (0.41 A mg^{-1} Pt) > Pt/C (0.32 A mg^{-1} Pt), indicating that oxidation current density for Pt@Heli-CeO_2/C is more than 3.1 times higher than that of Pt/C at the maximum in the forward sweep. The onset potential on ceria promoted Pt/C elecctrocatalysts are lower than that of Pt/C electrocatalyst in the forward sweep of the CV curves, suggesting that the performance of ceria promoted Pt/C electrocatalysts are superior to Pt/C.[49] Furthermore, the form of backward peaks on Pt@Heli-CeO_2/C, Pt@Octa-CeO_2/C and Pt/C are quite different. A relatively sharp peak is observed on Pt@Heli-CeO_2/C anode, corresponding to reoxidation of methanol or the removal of adsorbed carbonaceous species.[29] The chronoamperomentric *i-t* curves in N_2 saturated 0.5 M H_2SO_4 and 2.0 M CH_3OH aqueous solution at 0.5 V are presented in Figure 7b. For Pt@Heli-CeO_2/C, the current density at 3600 s is 0.089 A mg^{-1} Pt, approximately 8.2 times higher than that on Pt/C (0.011 A mg^{-1} Pt), and 3.3 times higher than that on Pt@Octa-CeO_2/C (0.027 A mg^{-1} Pt). This obviously enhanced oxidation activity for the Pt@Heli-CeO_2/C compared with Pt@Octa-CeO_2/C and Pt/C is definitely attributed to the enhancement in conductivity owing to the interfacial interaction between helical structured Heli-CeO_2 and Pt, attributed to the helical structured Heli-CeO_2 affording more active oxygen and exposing more active surface sites which is beneficial for the deposition of Pt nanoparticles. This in turn, increases the close contact and synergic interaction between Pt and helical structured Heli-CeO_2, reducing the aggregation of Pt, as well as the increased Pt (0) composition in Pt@Heli-CeO_2/C.

Conclusions

In summary, the results in the current study demonstrated a facile procedure to transform nano-octahedron CeO_2 to helical nanospindle Heli-CeO_2. The Heli-CeO_2 and Octa-CeO_2 promoted Pt/C samples were synthesized successfully by the microwave-assisted polyol synthesis method. Helical CeO_2 modified electrode exhibits higher activity than octahedron ceria supported electrode and Pt/C. The experimental results show that for methanol electro-oxidation Pt@Heli-CeO_2/C possesses 8.2 and 3.2 times higher activity than Pt/C and Pt@Octa-CeO_2/C, respectively. The significant enhancement for activity can be attributed to the follow reasons: (1) the unique helical structures are more conductive to electron transfer than the corresponding octahedral structure due to the intrinsic electronic structure; (2) more oxygen-containing species of helical structured Heli-CeO_2 support for Pt anchoring, and more active surface sites of helical structured CeO_2 to strengthen the support-metal interactions and promote homogenously dispersion of Pt crystallites; (3) reduced aggregation of Pt nanoparticles; (4) increased Pt (0) composition in helical CeO_2 supported electrode. The present study provides a new approach to design metal oxide cocatalyst for alcohol electrooxidation application.

Acknowledgements

The work was supported by the National Natural Science Foundation of China (Grant No. 51271012)

Notes and references

Key Laboratory of Aerospace advanced materials and performance of Ministry of Education, School of Materials Science and Engineering,

Beihang University, Beijing, 100191, P. R. China. E-mail: songmei_li@buaa.edu.cn; Tel.: +86 10 82317103.

Electronic Supplementary Information (ESI) available: TG result of CeO_2-Heli-P; H_2-TPR and N_2 adsorption-desorption isotherm results of obtained ceria. See DOI: 10.1039/b000000x/

1 Chu, Y. Y.; Wang, Z. B.; Jiang, Z. Z.; Gu, D. M.; Yin, G. P. *Adv. Mater.* 2011, **23**, 3100.
2 Ou, D. R.; Mori, T.; Togasaki, H.; Takahashi, M.; Ye, F.; Drennan, J. *Langmuir* 2011, **27**, 3859.
3 Zheng, J.; Cullen, D. A.; Forest, R. V.; Wittkopft, J. A.; Zhuang, Z.; Sheng, W.; Chen, J. G.; Yan, Y. *ACS Catal.* 2015, **5**, 1468.
4 Zhang, L.; Shen, Y. *ChemElectroChem* 2015, DOI: 10.1002/celc.201402432.
5 Kwak, D. H.; Lee, Y. W.; Han, S. B.; Hwang, E. T.; Park, H. C.; Kim, M. C.; Park, K. W. *J. Power Sources* 2015, **275**, 557.
6 Zignani, S. C.; Baglio, V.; Gonzalez, E. R.; Arico, A. S. *ChemElectroChem* 2014, **1**, 1403.
7 Wang, Y.; Wang, G.; Li, G.; Huang, B.; Pan, J.; Liu, Q.; Han, J.; Xiao, L.; Lu, J.; Zhuang, L. *Energy Environ. Sci.* 2015, **8**, 177.
8 Kakati, N.; Maiti, J.; Lee, S. H.; Jee, S. H.; Viswanathan, B.; Yoon, Y. S. *Chem. Rev.* 2014, **114**, 12397.
9 Ciftci, A.; Eren, S.; Ligthart, D. A. J. M.; Hensen, E. J. M. *ChemCatChem* 2014, **6**, 1260.
10 Nagao, R.; Freitas, R. G.; Silva, C. D.; Varela, H.; Pereira, E. C. *ACS Catal.* 2015, **5**, 1045.
11 Xu, D.; Bliznakov, S.; Liu, Z.; Fang, J.; Dimitrov, N. *Angew. Chem. Int. Edit.* 2010, **49**, 1282.
12 Liao, S. J.; Holmes, K. A.; Tsaprailis, H.; Birss, V. I. *J. Am. Chem. Soc.*2006, **128**, 3504.
13 Shen, Y.; Zhang, Z.; Xiao, K.; Xi, J. *ChemCatChem* 2014, **6**, 3254.
14 Huang, H.; Liu, Y.; Gao, Q.; Ruan, W.; Lin, X.; Li, X. *ACS Appl. Mater. Interfaces* 2014, **6**, 10258.
15 Ruiz-Camacho, B.; Rodriguez Santoyo, H. H.; Medina-Flores, J. M.; Alvarez-Martinez, O. *Electrochim. Acta* 2014, **120**, 344.
16 Shi, F.; Baker, L. R.; Hervier, A.; Somorjai, G. A.; Komvopoulos, K. *Nano Lett.* 2013, **13**, 4469.
17 Melvin, A. A.; Joshi, V. S.; Poudyal, D. C.; Khushaani, D.; Haram, S. K. *ACS Appl. Mater.Iinterfaces* 2015, **7**, 6590.
18 Zhang, W.; Sherrell, P.; Minett, A. I.; Razal, J. M.; Chen, J. *Energy Environ. Sci.* 2010, **3**, 1286.
19 Ho, V. T. T.; Pan, C. J.; Rick, J.; Su, W. N.; Hwang, B. J. *J. Am. Chem. Soc.* 2011, **133**, 11716.
20 You, E.; Guzmán-Blas, R.; Nicolau, E.; Aulice Scibioh, M.; Karanikas, C. F.; Watkins, J. J.; Cabrera, C. R. *Electrochim. Acta* 2012, **75**, 191.
21 Huang, S.; Chang, C.; Yeh, C. *J. Catal.* **2006**, 241, 400-406.
22 Takahashi, M.; Mori, T.; Ye, F.; Vinu, A.; Kobayashi, H.; Drennan, J. *J. Am. Ceram. Soc.* 2007, **90**, 1291.
23 Tan, Q.; Du, C.; Sun, Y.; Yin, G.; Gao, Y. *J. Mater. Chem. A* 2014, **2**, 1429.
24 Chu, Y. Y.; Cao, J.; Dai, Z.; Tan, X. Y. *J. Mater. Chem. A* 2014, **2**, 4038.
25 Xu, B.; Zhang, Q.; Yuan, S.; Zhang, M.; Ohno, T. *Appl. Catal. B: Environ.* 2015, **164**, 120.
26 Yu, X.; Kuai, L.; Geng, B. *Nanoscale* 2012, **4**, 5738.
27 Zagaynov, I. V.; Vorobiev, A. V.; Kutsev, S. V. *Mater. Lett.* 2015, **139**, 237.
28 Shen, G.; Liang, B.; Wang, X.; Chen, P. C.; Zhou, C. *ACS Nano* 2011, **5**, 2155.
29 Meher, S. K.; Rao, G. R. *ACS Catal.* 2012, **2**, 2795.
30 Peng, X.; Koczkur, K.; Nigro, S.; Chen, A. *Chem. Commun.* 2004, 2872.
31 Pozio, A.; De Francesco, M.; Cemmi, A.; Cardellini, F.; Giorgi, L. *J. Power Sources* 2002, **105**, 13.
32 Sui, X. L.; Wang, Z. B.; Li, C. Z.; Zhang, J. J.; Zhao, L.; Gu, D. M. *J. Power Sources* 2014, **272**, 196.
33 Lo Faro, M.; Reis, R. M.; Saglietti, G. G. A.; Sato, A. G.; Ticianelli, E. A.; Zignani, S. C.; Aricò, A. S. *ChemElectroChem* 2014, **1**, 1395.
34 Sui, X. L.; Wang, Z. B.; Li, C. Z.; Zhang, J. J.; Zhao, L.; Gu, D. M.; Gu, S. *J. Mater. Chem. A* 2015, **3**, 840.
35 Tarakeshwar, P.; Palma, J. L.; Holland, G. P.; Fromme, P.; Yarger, J. L.; Mujica, V. *J. Phys. Chem. Lett.* 2014, **5**, 3555.
36 Zheng, Y.; Lin, L.; Ye, X.; Guo, F.; Wang, X. *Angew. Chem. Int. Edit.* 2014, **53**, 11926.
37 Sun, S.; Zhang, G.; Geng, D.; Chen, Y.; Li, R.; Cai, M.; Sun, X. *Angew. Chem. Int. Edit.* 2011, **50**, 422.
38 Lee, E.; Manthiram, A. *J. Phys. Chem. C* 2010, **114**, 21833.
39 Carrasco, J.; López-Durán, D.; Liu, Z.; Duchoň, T.; Evans, J.; Senanayake, S. D.; Crumlin, E. J.; Matolín, V.; Rodríguez, J. A.; Ganduglia-Pirovano, M. V. *Angew. Chem. Int. Edit.* 2015, **127**, 1.
40 Ding, L. X.; Liang, C. L.; Xu, H.; Wang, A. L.; Tong, Y. X.; Li, G. R. *Adv. Mater. Interfaces* 2014, **1**, DOI: 10.1002/admi.201400005.
41 Wang, X.; Liu, D.; Song, S.; Zhang, H. *J. Am. Chem. Soc.* 2013, **135**, 15864.
42 Jiang, Z. Z.; Wang, Z. B.; Qu, W. L.; Gu, D. M.; Yin, G. P. *Appl. Catal. B: Environ.* 2012, **123-124**, 214.
43 Haber, J. A.; Anzenburg, E.; Yano, J.; Kisielowski, C.; Gregoire, J. M. *Adv. Energy Mater.* 2015, DOI: 10.1002/aenm.201402307.
44 Zhou, Y.; Lawrence, N. J.; Wu, T. S.; Liu, J.; Kent, P.; Soo, Y.-L.; Cheung, C. L. *ChemCatChem* 2014, 6, 2937.
45 Larachi, F. ç.; Pierre, J.; Adnot, A.; Bernis, A. *Appl. Surf. Sci.* 2002, **195**, 236.
46 Aricò, A. S.; Shukla, A. K.; Kim, H.; Park, S.; Min, M.; Antonucci, V. *Appl. Surf. Sci.* 2001, **172**, 33.
47 Yin, A. X.; Min, X. Q.; Zhu, W.; Wu, H. S.; Zhang, Y. W.; Yan, C. H. *Chem. Commun.* 2012, **48**, 543.
48 Wang, X.; Li, X.; Liu, D.; Song, S.; Zhang, H. *Chem. Commun.* 2012, **48**, 2885.
49 Hofstead-Duffy, A. M.; Chen, D.-J.; Sun, S. G.; Tong, Y. J. *J. Mater. Chem.* 2012, **22**, 5205.

GRAPHICAL ABSTRCT